RSC Advances

ROYAL SOCIETY OF CHEMISTRY

www.rsc.org/advances

Thermal Degradation Behavior of Flame Retardant Melamine Derivative Hyperbranched Polyimide with Different Terminal Groups

Muhammad Bisyrul Hafi **Othman**[1], Zulkifli **Ahmad**[1], Hasnah **Osman**[2], Mohd Firdaus **Omar**[3] and Hazizan **Md Akil**[1]*

[1]School of Materials and Mineral Resources Engineering, Engineering Campus, Universiti Sains Malaysia Seri Ampangan, 14300 Nibong Tebal Pulau Pinang, Malaysia

[2]School of Chemical Sciences, Universiti Sains Malaysia, 11800 Minden Pulau Pinang, Malaysia

[3]CEGeoGTech, School of Material Engineering, Universiti Malaysia Perlis, Kompleks Pengajian Jejawi2, 02600 Arau Perlis, Malaysia

*Corresponding author: hazizan@usm.my

Tel: +604 599 6161

Fax : +604 594 1011

Abstract

Melamine derivative hyperbranched polyimide (HPI) with different terminal groups were synthesized by emulsion polymerization reactions and followed by stepwise thermal imidization. The non-isothermal behavior of synthesized HPI polymers was studied by thermogravimetric analysis under nitrogen atmosphere and the results were compared with the corresponding terminal groups. In this study, the researchers attempted to clarify the effects of different terminal groups on the non-isothermal degradation kinetics. The chosen apparent activation energy using Flynn-Wall-Ozawa and Kissinger methods shows that it fits with each other (same trend). Meanwhile, the type of solid state mechanism was determined using the Coats-Redfern and Criado methods proposed for D1 types such as amine-amine terminals, amine-anhydride terminals and anhydride-anhydride terminals, which are one-dimensional diffusions that follow the unimolecular decay law with the first order reactions. The E_a showed significant differences at $\alpha > 0.7$, which indicates the role of different terminal groups towards degradation behavior. From the calculations, the lifetime prediction at 5% mass loss decreases in the following order: anhydride terminated > amine terminated > anhydride-amine terminated which is related to the dissociation energy between the anhydride functional groups and amine functional groups. Hence, the presence of different terminal groups reveals their contributions towards thermal degradation and stability.

Keyword: thermal properties; thermal stability; kinetic degradation; activation energy (E_a); lifetime.

Nomenclatures (SI unit)/ Abbreviation

3D	Three-dimensional
α	Conversion
β	Heating rate; ($Kmin^{-1}$)
$d\alpha/dt$	Rate of conversion
$d^2\alpha/dt^2$	Rate of conversion for second derivative thermogravimetry
$f(\alpha)$	Expression of kinetic model
A	Pre-exponential factor (min^{-1})
ASTM	American Society for Testing and Materials
BPDA	4,4'-(4,4'-Isopropylidenediphenoxy) bis(phthalic anhydride)
c	Intercept-y
C-Red	Coats-Redfern
DDTG	Second derivative thermogravimetry
DMF	Dimethylformamide
DSC	Differential scanning calorimetry
DTG	Derivative thermogravimetry
E_a	Activation energy ($kJmol^{-1}$)
Eq	Equation
F-W-O	Flynn-Wall-Ozawa
$g(\alpha)$	Integral form of the conversion function
H-Mat	Horowitz-Metzger
HCl	Hydrochloric acid
HPI	Hyperbranch polyimide
k	Rate constant
MB11	Anhydride-amine terminated
MBX1	Amine terminated
MB1X	Anhydride terminated
Mac-T	MacCallum-Tanner
M_o	Initial mass (g)
M_t	Mass at time (g)
M_f	Final mass (g)
Mw	Mass average molar mass ($gmol^{-1}$)
n	Kinetic order.
N_2	Nitrogen gas
NMP	N-methylpyrolidone
T_5	Temperature at 5% mass loss (K)
T_{10}	Temperature at 10% mass loss (K)
R	Gas constant ($8.314\ Jmol^{-1}\ K^{-1}$)
R_w	Residue mass (g)
T_d	Temperature at maximum mass loss (K)
TG	Thermogravimetry
Tg	Glass transition temperature
t	Time (min)
$Z(\alpha)$	Integral form of the model of kinetic function

1. Introduction

The synthesis of hyperbranched polyimide (HPI) has been widely reported over the past decade due to the system's ability to demonstrate good physical, chemical, and thermal properties required for those seeking to improve and counterbalance solubility and processability and simultaneously maintaining the thermal stability of the HPI material [1, 2]. For these reasons, in this study, S-triazine moieties have been added into the HPI backbone to improve the properties stated above, especially regarding the balance of polyimide properties in a fully imidized form. 1,3,5-triazine (known as melamine) is the most readily available and inexpensive monomer to reinforce the s-triazine units, and thus, is suitable for research and commercialization. The presence of s-triazine units from melamine will be able to maintain the thermal properties of HPI due to the properties of melamine itself as a fire retardant.

Many studies have been conducted to obtain desirable properties for potential industrial applications, such as modification of HPI structure by chemical methods and with other moieties[2-4]. However, the utilization of melamine in HPI backbones is quite new, and only a little work devoted to its synthesis has been reported. Additionally, the contribution of its derivatives towards kinetic degradation and thermal stability in the resulting properties from different terminal groups on the lifetime of HPI systems is not well explored. Rauch and Fanelli [5] studied the thermal decomposition kinetics of hexahydro-1, 3, 5-trinitro-s-triazine above the melting point to provide an evidence for both gas and liquid phase decompositions. Yang *et al.* [6] studied a trifunctional phenylethynyl-terminated imide oligomer by using TGA and DSC methods and then identified the rheological behaviour and cure kinetics. The latest study from Gosh *et al.* [7]

reviewed the synthesis and applications of an aromatic HPI polymer without mentioning any kinetic parameters and solid states involved.

Nevertheless, the solid state thermal mechanism and kinetics of 1,3,5-triazine-2,4,6-triamine (melamine)/ 4,4'-(4,4'-isopropylidenediphenoxy) bis(phthalic anhydride) (BPDA) HPI have not been studied before. On the other hand, the utilization of S-triazine moieties in HPI is known to improve the processability of polyimide polymers. Thus, in this paper, the researchers attempted to provide several findings that will address the basics of kinetic degradation. It is already known from previous experience that kinetic analysis based on single heating rate (β) methods (isothermal) is not dependable and many problems have been encountered [8]. Therefore, multiple heating rate methods (non-isothermal) such as Flynn-Wall-Ozawa (F-W-O) [9-11], Kissinger [12, 13], Coats-Redfern (C-Red) [14-16], Horowitz-Metzger (H-Met) [17], MacCallum-Tanner (Mac-T) [18, 19], van Krevelen [20], Friedman [21] and others are more preferred for the same reason. Non-isothermal approaches are found to be more convenient to carry out because it is not necessary to perform a sudden temperature elavation of the sample at the beginning of the experiment.

Finally, it should be very interesting to understand the structure-properties relationship that is governed by the mathematical description of the decomposition process of polymers in a solid state. The process relies on three kinetic components; (1) two Arrhenius parameters, apparent activation energy (E_a) and pre-exponential factor (A); (2) the analytical expression describing the kinetic model, $f(\alpha)$; and (3) the former parameter E_a, all of which are the most frequently used parameters to discuss the thermal stability of these polymers. The kinetic degradation and glass transition temperature, as well as chain mobility that have been obtained from TGA and DSC analysis can generate

parameters, which can be subsequently used to deduce the lifetime of polymers at different temperatures. The thermal behavior of the HPI system is reported to depend on the three-dimensional (3D) form of the cross-linked polymeric network [8]. However, HPI with different terminal group systems has not been reported previously. Besides that, different terminal groups of HPI will generate different thermal characteristics, which are due to the changes occurring in their chemical structures, as well as changes in their environment.

The present paper deals with the comparative non-isothermal degradation kinetic study of different terminal groups of melamine HPI derivatives. The apparent E_a was determined using the F-W-O, Kissinger and C-Red methods. The data presented in this study will be very useful for the investigators to estimate and distinguish the lifetime of a PI system qualitatively or quantitatively. In addition, this study aims to collectively link the methods that have been previously studied in isolation from each other into a comprehensive context, as well as providing more useful information on a wide range of related areas. The type of solid state mechanism was determined using the Criado method [22-24] that uses the F-W-O kinetic data at low conversions based on Doyle approximations[25-27]. The kinetic parameter (rate constant k; E_a) was calculated and subsequently employed to predict the influence of different terminal groups of melamine HPI on its lifetime. All different terminal groups of melamine HPI were derived from melamine monomers prepared through the emulsion polymerization method in an acidic medium at room temperature and followed by thermal imidization.

2. Theoretical

In order to determine the kinetic parameters such as reaction order (η), E_a, and others, thermogravimetric (TG) analysis is applied. The rate of reaction can be defined as the ratio of actual mass loss at time (t) to the total mass loss at complete degradation process as shown in (Eq. 1) [28].

$$\alpha = \frac{M_o - M_t}{M_o - M_f} \qquad (1)$$

where M_o, M_t, and M_f, are the initial mass of sample, the mass of sample at time *t*, and the final mass, respectively, of the completely decomposed sample.

Generally, a typical model for a kinetic process of polymer degradation can be represented by the decomposition rate ($d\alpha/dt$), which is a function of temperature and mass of the sample. It is assumed that the rates of conversion (α) are proportional to the concentration of the reacted material. Thus, the rate of α can be expressed by the following basic rate equation (Eq. 2).

$$\frac{\mathrm{d}\alpha}{\mathrm{d}t} = k(T) f(\alpha) \qquad (2)$$

where $d\alpha/dt$ is the degradation rate, k is the rate constant, and $f(\alpha)$ is the differential expression of a kinetic model function. However, k is given by the Arrhenius Equation (Eq. 3) expression:

$$\mathrm{k} = \mathrm{A}\exp - \frac{Ea}{RT} \qquad (3)$$

where A is the frequency factor (s^{-1}), E_a is the apparent kinetic energy of the degradation reaction ($kJmol^{-1}$), R is the gas constant, α and T is the absolute temperature. It can be assumed that k from (Eq. 1) follows the Arrhenius Equation. Thus, substituting (Eq. 3) into (Eq. 1), one obtains (Eq. 4).

$$\frac{\mathrm{d}\alpha}{\mathrm{d}t} = A\exp\left(-\frac{Ea}{RT}\right)\mathrm{f}(\alpha) \qquad (4)$$

According to the non-isothermal kinetic theory, thermal degradation data is generally performed using the following (Eq. 5).

$$\frac{\mathrm{d}\alpha}{\mathrm{d}t} = \beta\frac{d\alpha}{dT} = A\exp\left(-\frac{Ea}{RT}\right)\mathrm{f}(\alpha) \qquad (5)$$

where $\beta=dT/dt$ is a constant. Rearranging (Eq.5), one can simplify the equation into (Eq. 6).

$$\frac{\mathrm{d}\alpha}{\mathrm{d}t} = \frac{A}{\beta}\exp(-\frac{Ea}{RT})f(\alpha) \qquad (6)$$

where $f(\alpha)$ is the differential expression of a kinetic model function, β is the heating rate (K/min), E_a and A are respectively the E_a ($kJmol^{-1}$) and pre-exponential factor (min-1) for the decomposition reaction, with R as the gas constant (8.314 $Jmol^{-1}$ K^{-1}). Generally, E_a can be calculated by using either the F-W-O, Kissinger, C-Red, H-Mat, Mac-T, or van Krevelen methods. However, the F-W-O, Kissinger and C-Red are the superior methods

for dynamic heating experiments, as the calculation of E_a does not consider η. Thus, only these three methods are taken further into discussion.

2.1 Flynn-Wall-Ozawa; F-W-O method (integration method) [9-11]

F-W-O method can be used to quantify E_a without any knowledge of the reaction mechanism. The method is not based on any assumptions concerning the temperature integral, thus giving a higher degree of precision to the results. Therefore, this method [14] is a free model technique that evaluates the dependence of the effective E_a on α. Besides that, this method is very useful for kinetic interpretations of TG data obtained from complex reactions. Using (Eq. 6), the data can be integrated using the Doyle approximation [25-27]. The result of the integration after taking logarithms is either (Eq. 7a) or (Eq. 7b).

$$\log \beta = \log \frac{AE_a}{g(\alpha)R} - 2.315 - \frac{0.457E_a}{RT} \qquad (7a)$$

or

$$\ln \beta = \ln\left(\frac{AE_a}{R}\right) - \ln g(\alpha) - 5.3305 - \frac{1.052E_a}{RT} \qquad (7b)$$

where E_a of the thermal degradation process PI with different terminal groups is determined from the slope of the straight line log β versus 1/T.

2.2 Kissinger method (differential method) [12, 13]

Kissinger method uses Eq. (8) to determine the E_a of solid state reactions.

$$\ln\left(\frac{\beta}{T_p^2}\right) = \ln\frac{AR}{E_a} + \ln\left[n\left(1-\alpha_p\right)^{n-1}\right] - \frac{E_a}{RT} \qquad (8)$$

where T_p and α_p are the absolute temperature and mass loss at maximum mass loss rate $(d\alpha/dt)_p$, respectively, and n is the reaction order. From the slope of the straight line ln (β/T_p^2) versus $1/T_p$, the E_a can be obtained. The advantage of Kissinger model is that the E_a can be obtained without prior knowledge of any thermal degradation reaction mechanism.

2.3 Coats-Redfern (C-Red) method [14-16]

Based on integral models, $g(\alpha)$, C-Red equation (Eq. 9) has been used to estimate the Arrhenius parameters. However, this method is unable to reveal the complexities of the process, in which the obtained average value of parameters do not reflect changes in the mechanism and kinetics regarding the temperature and α.

$$\ln\frac{g(\alpha)}{T^2} = \ln\left[\frac{AR}{\beta E_a}\left(1-\frac{2RT}{E_a}\right)\right] - \frac{E_a}{RT} \qquad (9)$$

Considering using Doyle approximation that $ln\ (1 - 2RT/ E_a) \rightarrow 0$, (Eq. 9) is written as (Eq. 10).

$$\ln\frac{g(\alpha)}{T^2} = \ln\left(\frac{AR}{\beta E_a}\right) - \frac{E_a}{RT} \qquad (10)$$

By inserting different forms of $g(\alpha)$ into (Eq. 9), the results are obtained in a set of Arrhenius parameters. The linear plot of $ln[g(\alpha)/T^2]$ versus 1/T makes it possible to determine E_a and $ln(A)$ from the slope and intercept of the graph, respectively. It has been shown in some studies that the analytical model fitting method is unreliable and tends to yield meaningless kinetic parameters [8]. Furthermore, the solid state reactions are sensitive to many factors, which are likely to change during the process. Model-fitting methods (such as C-Red method) are designed to extract a single set of Arrhenius parameters for the whole conversion ranges.

2.4 Determination of the reaction mechanism using Criado method [22-24]

The degradation reaction mechanism can be determined using Criado method. Criado *et al*. [23] proposed a method that can accurately determine the reaction mechanism in solid reaction processes and define a type of Z(a) in a function as written in Eq. (11):

$$Z(\alpha)=\frac{\left(\frac{d\alpha}{dt}\right)}{\beta}\pi(x)T \qquad (11)$$

where x = E_a/RT and π(x) via an approximate expression by integration against temperature, which cannot be expressed by using any simple analysis formula [29]. A reasonable relationship between π(x) and P(x) is $\pi(x)=xe^{x}P(x)$,where P(x) is as shown in Eq. (12), which is proposed by Senum and Yang [30].

$$P(x)=\frac{e^{-x}}{x}\frac{x^3+18x^2+86x+96}{x^4+20x^3+120x^2+240x+120}$$

When x>20, the error of Eq is less than 10-5%, which is the basis that will be used in this paper.

By combining (Eq. 1), (Eq. 11) and (Eq. 12), (Eq. 13) is obtained.

$$Z(\alpha) = f(\alpha)g(\alpha) \qquad (13)$$

Thus, the relationship between (Eq. 1) and (Eq. 11) can be derived as (Eq. 14).

$$Z(\alpha) = \frac{d\alpha}{dT}\frac{Ea}{R}e^{Ea/RT}P(x) \qquad (14)$$

To study the mechanism of materials, various expressions of differentials, *f(α)*, integral form of the conversion function, *g(α)*, and forms of different solid state mechanisms, Eq. (13) is used to plot the master *Z(α)-α* curves for different models listed in **Table 1**. Eq. (14) is used to represent the experimental curve. The mechanism type and solid state of thermal degradation can be identified by comparing these two curves.

Table 1
for *g(α)* and *f(α)* for the most frequently used mechanisms of solid state processes.

Mechanism	S	*g(α)*	*f(α)*
Nucleation and growth (Avrami equation (1))	A2	$[-\ln(1-\alpha)]^{1/2}$	$2(1-\alpha)[-\ln(1-\alpha)]^{1/2}$
Nucleation and growth (Avrami equation (2))	A3	$[-\ln(1-\alpha)]^{1/3}$	$3(1-\alpha)[-\ln(1-\alpha)]^{1/3}$
Nucleation and growth (Avrami equation (3))	A4	$[-\ln(1-\alpha)]^{1/4}$	$4(1-\alpha)[-\ln(1-\alpha)]^{1/4}$
Phase boundary controlled reaction (one-dimensional movement)	R1	α	1
Phase boundary controlled reaction (contracting area)	R2	$[1-(1-\alpha)]^{1/2}$	$2(1-\alpha)^{1/2}$
Phase boundary controlled reaction (contracting volume)	R3	$[1-(1-\alpha)]^{1/3}$	$3(1-\alpha)^{1/3}$
One-dimensional diffusion	D1	α^2	$(1/2)\alpha 1^{-1}$
Two-dimensional diffusion (Valensi equation)	D2	$(1-\alpha)\ln(1-\alpha)+\alpha$	$-[\ln(1-\alpha)^{-1}$
Three-dimensional diffusion (Jander equation)	D3	$[1-(1-\alpha)^{1/3}]^2$	$(3/2)[1-(1-\alpha)^{1/3}]^{-1}-(1-\alpha)^{2/3}$

Three-dimensional diffusion (Ginstling Brounshtein equation)	D4	$[1-(2/3\ \alpha)^{1/3}]-(1-\alpha)^{2/3}$	$(3/2)[1-(1-\alpha)^{1/3}]^{-1}$
Random nucleation with one nucleus on the individual particle	F1	$-\ln(1-\alpha)$	$1-\alpha$
Random nucleation with two nuclei on the individual particle	F2	$1/(1-\alpha)$	$(1-\alpha)^2$
Random nucleation with three nuclei on the individual particle	F3	$1/(1-\alpha)^2$	$(1-\alpha)^3$

3. Experimental

3.1. Materials

1,3,5-triazine-2,4,6-triamine (Melamine; 98%) and 4,4'-(4,4'-isopropylidenediphenoxy) bis(phthalic anhydride) (BPDA; 98%) used as monomers were purchased from Alfa Aesar USA, where they were used as received without further purification. Dimethylformamide (DMF) and N-methyl-2-pyrrolidone (NMP) used as solvents were distilled over calcium hydride under nitrogen flow and stored with a molecular sieve (Type 4A, Aldrich) before being used. Hydrochloric acid (HCPolyimil) used as the emulsifier agent, along with the solvents mentioned above, were purchased from Merck Darmstadt, Germany.

3.2. Synthesis of an aromatic HPI

All the reported HPI series containing s-triazine rings in the main chain were derived from melamine and BPADA. The synthesis was successful conducted via emulsion polymerization according to the A3 + B2 approach as summarized in **Table 2**. The conventional two-step method details have been reported in other studies [31]. While the proposed chemical structure of HPI based on melamine as S-triazine unit's shows in **Fig. 1**.

Table 2
Summarisation of controlled parameters.

Melamine (A3)	BPADA (B2)	DMF	HCl	Temperature	Time	Sample

mol (mass, g)	*mol (mass, g)*	*mL*	*mL*	*°C*[a]	*h*	
0.020 (2.54)	0.030 (15.62)	80.0	10.0	Ambient [a]	24	MB11
0.028 (3.54)	0.030 (15.62)	80.0	10.0	Ambient [a]	24	MBX1
0.020 (2.54)	0.032 (16.62)	80.0	10.0	Ambient [a]	24	MB1X

[a] The reaction performed at temperature within 27 – 29 °C

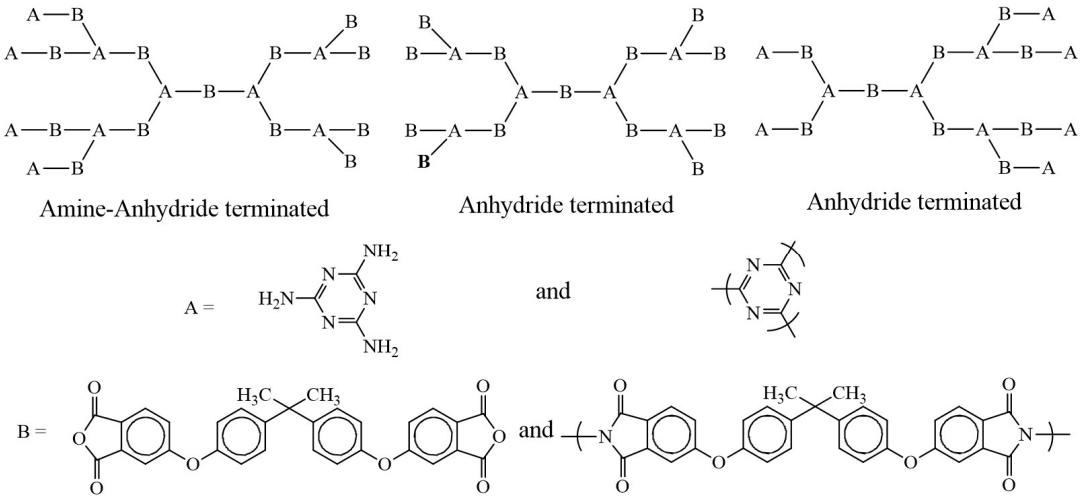

Fig. 1. The proposed chemical structure of HPI based on melamine as triazine units.

MB11: Anhydride-amine terminated: GPC analysis: Mn = 16000 - 19000, Mw = 19000 – 25000, Mz = 23000 - 31000, PD = 1.21 – 128. FTIR spectrum (powder): νmax= 1780 cm−1 and 1724 cm−1 (unsymmetrical C=O of imide and Symmetrical C=O of imide stretches), 1374 (C–N of imide stretch), 1102 cm−1 and 747 cm−1 (imide ring deformation), 1100–1300 cm−1 (C–O stretching), 723 (C-N-C of imide ring formation). FTIR 1H-NMR (400 Hz, DMSO): δ (ppm) 8.08 (Ha, doublet), 7.68 (Hb, doublet), 7.00 – 7.50 (singlet/doublet, Hc, Hd, He, Hf, Hg), 6.99 (2Hh, singlet), 1.69 (6Hi, singlet).[31]

MBX1: Amine terminated: GPC analysis: Mn = 16000 - 19000, Mw = 19000 – 25000, Mz = 23000 - 31000, PD = 1.21 – 128. FTIR spectrum (powder): νmax= 1780 cm−1 and 1724 cm−1 (unsymmetrical C=O of imide and Symmetrical C=O of imide stretches), 1374 (C–N of imide stretch), 1102 cm−1 and 747 cm−1 (imide ring deformation), 1100–1300 cm−1 (C–O stretching), 723 (C-N-C of imide ring formation). FTIR 1H-NMR (400 Hz, DMSO): δ (ppm) 8.08 (Ha, doublet), 7.00 – 7.50 (singlet/doublet, Hc, Hd, He, Hf), 6.99 (2Hh, singlet), 1.69 (6Hi, singlet).[31]

MB1X: Anhydride terminated: GPC analysis: Mn = 16000 - 19000, Mw = 19000 – 25000, Mz = 23000 - 31000, PD = 1.21 – 128. FTIR spectrum (powder): νmax= 1780 cm−1 and 1724 cm−1 (unsymmetrical C=O of imide and Symmetrical C=O of imide stretches), 1374 (C–N of imide stretch), 1102 cm−1 and 747 cm−1 (imide ring deformation), 1100–1300 cm−1 (C–O stretching), 723 (C-N-C of imide ring formation). FTIR 1H-NMR (400 Hz, DMSO): δ (ppm) 8.08 (Ha, doublet), 7.68 (Hb, doublet), 7.00 – 7.50 (singlet/doublet, Hc, Hd, He, Hf, Hg), 1.69 (6Hi, singlet).[31]

3.3. Characterizations

The final chemical structure of terminal groups present in the HPI were identified using the Fourier transform infrared (Spectrum GX Perkin Elmer Model) and proton-nuclear magnetic resonance (Bruker 400 Ultra Shield TM Model), which have previously been reported in other studies [31].

3.4 Thermal analysis

Different scanning calorimetry (DSC) analysis was performed by using a DSC-6 analyzer (Perkin Elmer; Norwalk, CT, USA) at β 10 ^{o}Cmin-1 in nitrogen from 30 °C to 340 °C to measure the glass transition temperature (T_g). The dynamic and non-isothermal thermogravimetric (TG) analysis was conducted using a Pyris 6 TGA thermogravimetric analyzer (Perkin Elmer; Norwalk, CT, USA). About 10 mg of the sample was placed in an aluminum crucible and heated from room temperature to 800 °C with a heating rate of 5, 10, and 20 ^{o}Cmin^{-1} in nitrogen atmosphere. The mass loss versus temperature was recorded. The onset decomposition temperature (T_d), 10% mass loss temperature (T_{10}) and residual mass (Rw) at 800 °C were also determined. Finally, the kinetic analyses via F-W-O, Kissinger and C-Red methods were carried out at various β, i.e. 5, 10, and 20 °Cmin^{-1}. The type of solid state mechanism was determined by the Criado method using F-W-O kinetic data at a low conversion ($\alpha \leq 30$ %) based on Doyle approximations.

4. Results and discussion

4.1. Characteristics of the HPI

In our previous published work [31], the chemical structure of the synthesized HPIs' melamine derivative was confirmed to display imide characteristics between 1780 cm−1

and 1724 cm−1 (unsymmetrical C=O of imide and symmetrical C=O of imide stretches), 1374 (C–N of imide stretch), 1102 cm−1 and 747 cm−1 (imide ring deformation) and 723 (C-N-C of imide ring formation), together with strong absorption bands around 1100–1300 cm−1 due to C–O stretching. As expected, thermal imidization did not affect the backbone's main characteristics, which remained at -$C(CH_3)_2$ and C-O-C. The HPI series was imidized more than 80% above 180 °C and had Mw between 21000 to 23000 $gmol^{-1}$, while PD was in the 1.2 range. The glass transition temperature (Tg) of HPIs was determined by using DSC analysis during the second heating process at a β of 10 $^{o}Cmin^{-1}$ and was found to exceed 190 ^{o}C (**Fig. 2**), which demonstrates an acceptable range to be used for high performance polymers for processability and stability

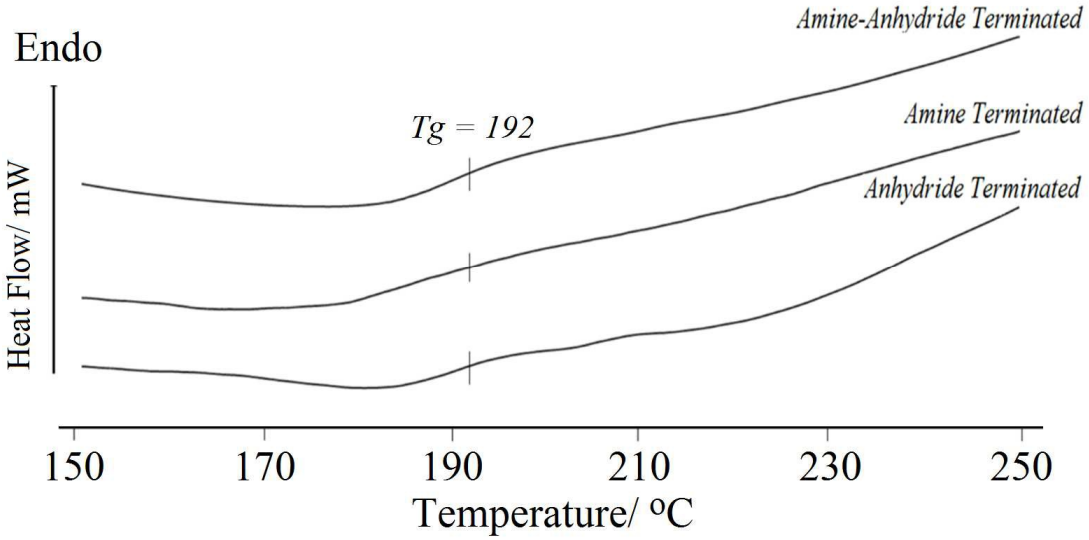

Fig. 2. DSC trace for thermal glass transition temperature T_g of some HPI series derived from BAPP/BPDA monomers in nitrogen atmosphere for different types of silicone segment treated.

Thermal stability of HPI was evaluated using TG analysis in nitrogen atmosphere β values of 5, 10, and 20 $^{o}Cmin^{-1}$. The mass loss versus temperature curve of thermal

degradation of melamine HPI based on the corresponding types of terminal groups was obtained at different βs as shown in **Fig. 3**.

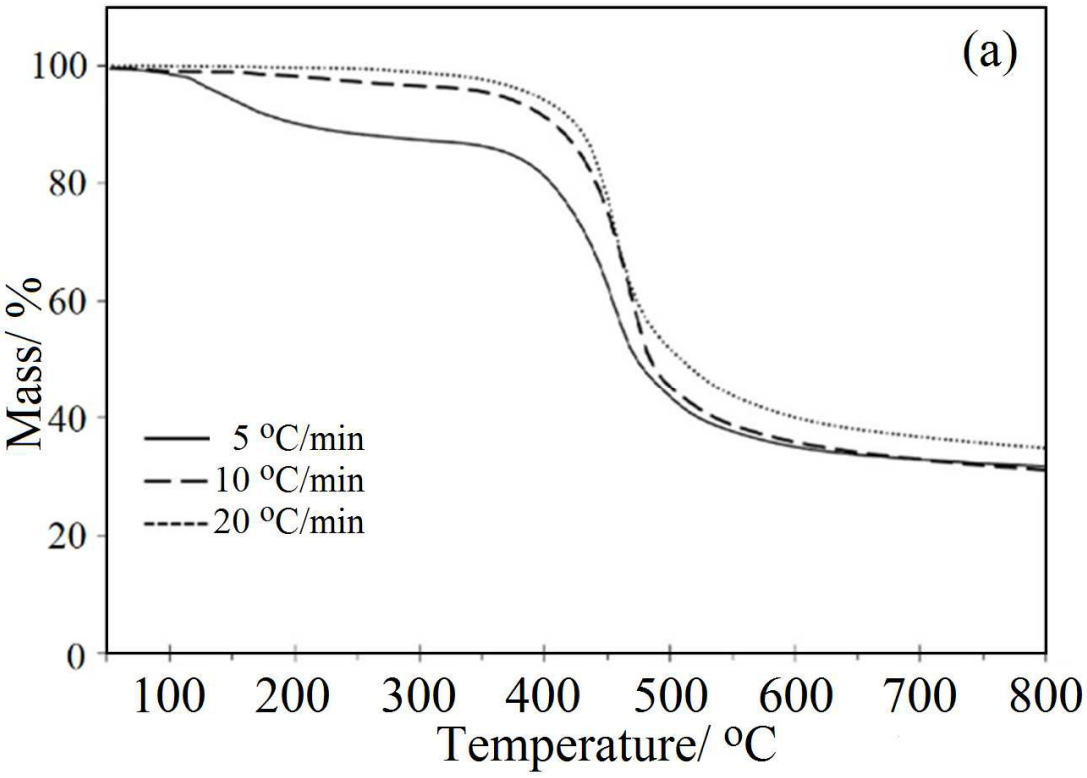

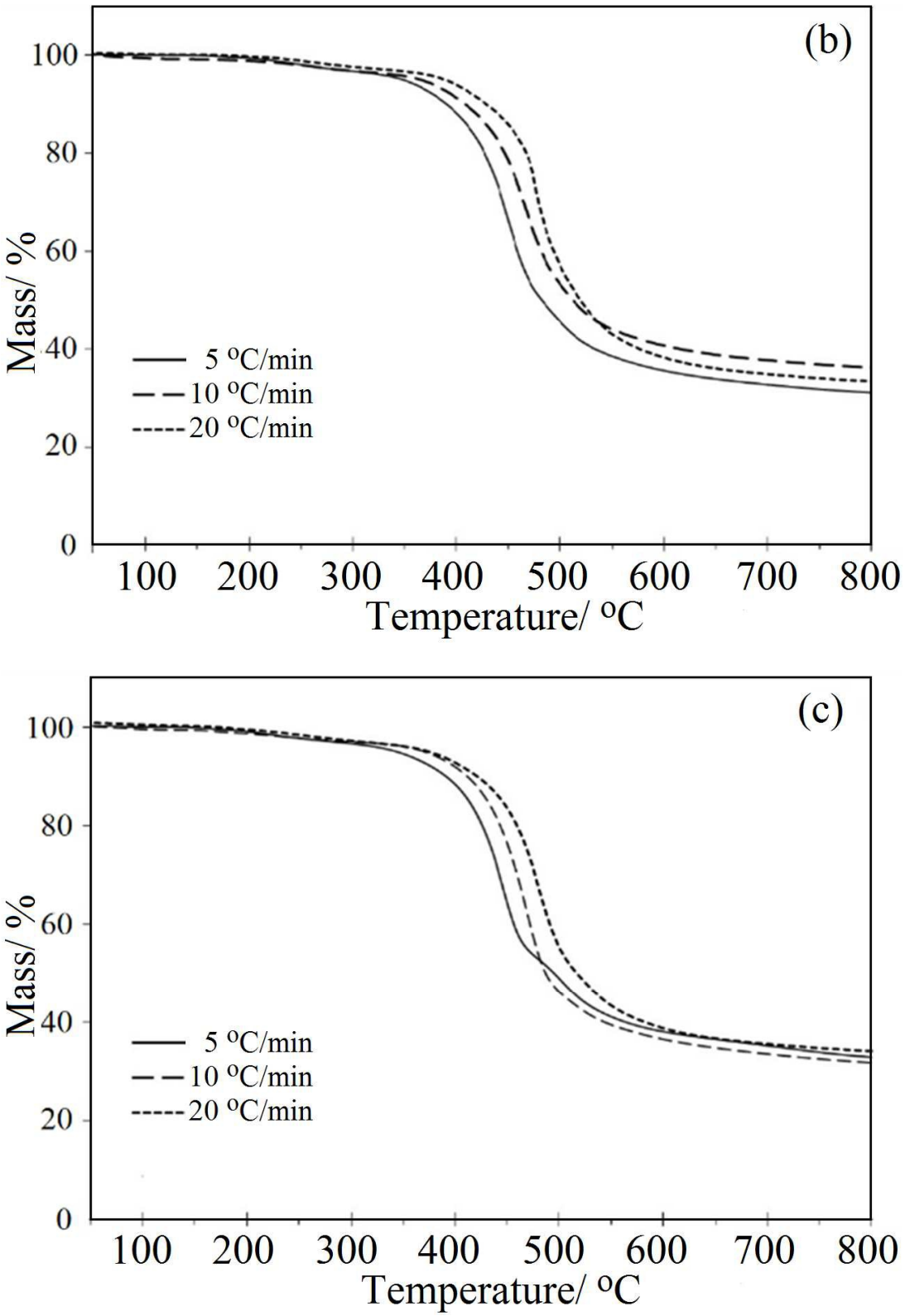

Fig. 3. Variation of mass loss versus temperature at different β (a) anhydride-amine terminated, (b) amine terminated and (c) anhydride terminated.

The 5 ^{o}C min^{-1} is considered as low β (**Fig 3a**), thus the time of attainment for the thermodynamic equilibrium is sufficient enough to initiate several supplementary reaction which include dehydration from terminated amine with anhydride within HPI chain. The step occurred at 5 ^{o}C min^{-1}, variably suggested is due to decomposition of water including supplementary dehydration reaction between amine and anhydride group. This has been proven by Xie et al [32] in his study on thermal analysis combined with evolved gas analysis (TG/FTIR). Interestingly, they found that the water region at temperatures below 200°C. However at higher β, the interval is not sufficient to attain thermodynamic equilibrium of the system which is favor any inducing of supplementary reaction such as dehydration of water molecules. This otherwise could not similarly observed for the step degradation at region 150 ^{o}C at 10 and 20 ^{o}C min^{-1}

These figures showed a major decomposition at 400 °C and there was more than 30% residue once the degradation was completed at 800 °C. The curve was delayed and shifted to higher temperatures as the β increased from 5 to 20 °C/min. From **Fig. 3 (a-c)**, it is evident that the thermal decomposition of samples was in the range of 100-800 °C. At higher βs, the system does not have sufficient time to attain thermodynamic equilibrium, thus inducing higher thermal stress. Under the viscoelastic system of polymeric structures, a low β will induce higher thermal stress since it is able to supply and induce bond vibrations efficiently around its thermodynamic equilibrium, and as a result, T_d will occur at lower temperatures. On the other hand, at a higher β, the thermal stress is not sufficiently accumulated. This results in no deviation of its thermodynamic equilibrium, yet the system degrades at higher temperatures. Meanwhile, for comparison purpose, the thermal degradation of melamine HPI corresponding to the same βs at different types of terminal groups is shown in **Fig. 4**.

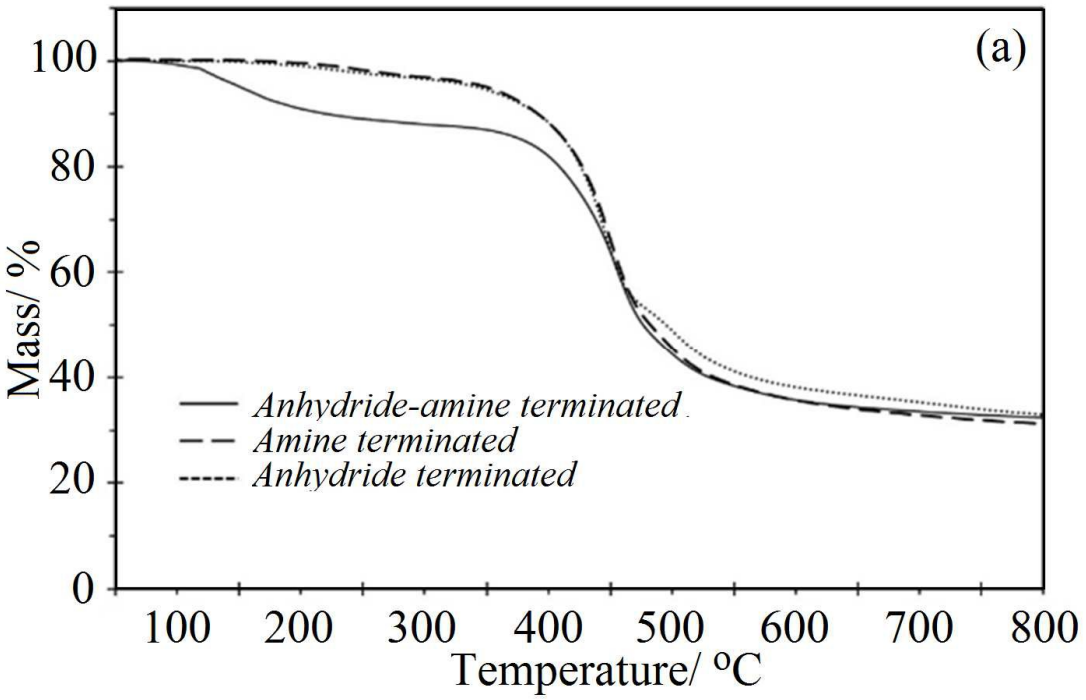

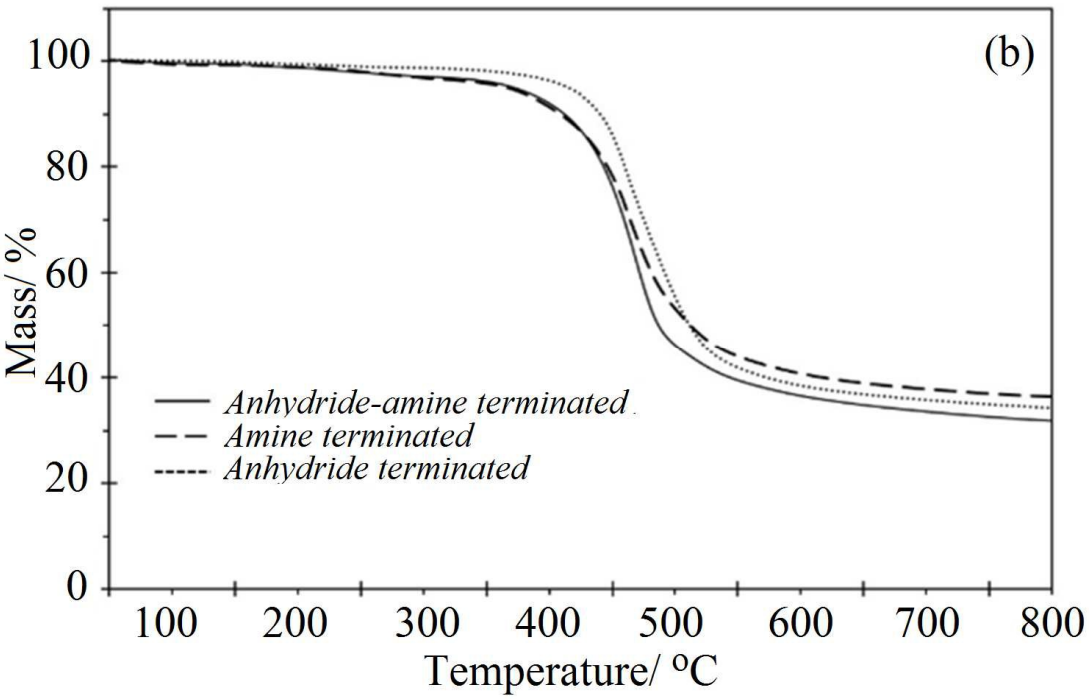

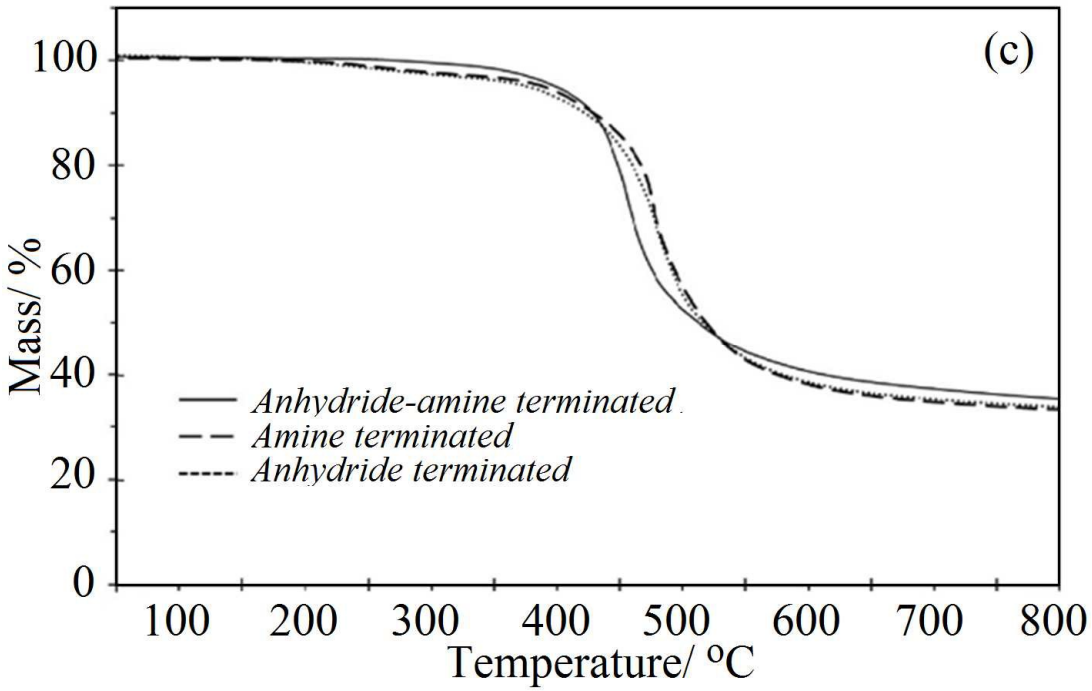

Fig. 4. Comparison of mass loss for different terminal groups at **(a)** β = 5 °C/min **(b)** β = 10 °C/min and **(c)** β = 20 °C/min

Although the curves in **Fig.4 (a-c)** did not show any significant changes with the change of terminal groups, it is clear that the curves displayed did not overlapped. These are evidence that the terminal groups have contributed to the stability during thermal degradation, either thermodynamically or kinetically, that will be reason to evaluate here. **Table 3** summarizes the TG traces of HPI with different terminal groups in nitrogen atmosphere.

Table 3
Result of TG traces of some PI film in nitrogen atmosphere.

Sample Designation	**β**	**Char Residue** [a]	**$T_{10\%}$** [°C][e]	**T_{onset}** [°C][b]	**T_{max}** [°C][c]	**T_{end}** [°C][d]	**ΔT** [°C][f]
Anhydride-amine terminated	5	32.4	221	385	452	545	160
	10	31.8	410	392	465	540	150
	20	35.5	428	382	468	550	168
	Average	33.2	353	386.3	461.7	545	159.3
Amine-terminated	5	31.3	391	350	448	548	198
	10	32.9	409	365	471	542	197
	20	36.4	429	380	482	560	180

	Average	32.9	409.7	365	467	550	191.7
Anhydride terminated	5	32.9	391	360	442	554	194
	10	31.8	412	368	458	564	196
	20	34.1	422	378	484	576	198
	Average	32.9	408.3	368.7	461.3	564.7	196.0

[a] wt % residue at 800 ^{o}C, [b] Onset temperature of degradation, [c] Temperature of maximum rate of mass loss, [d] End temperature of degradation, [e] Temperature corresponding to percentage of mass loss, [f] $\Delta \mathbf{T} = \mathbf{T}_{end} - \mathbf{T}_{onset}$, [g] Integral procedural decomposition temperature.

From **Table 3**, the average char residue for all samples was about 33% once the degradation was completed at 800 °C. This means that the presence of different terminal groups in the HPI system, thermodynamically does not contribute much to the changes in thermal stability. Therefore, these findings suggest that the molecule architecture consists of the same repeated unit. Even though each HPI series has different terminal groups, the findings still show the same decomposition as thermodynamic stability. This synergy in the char formation was observed in the system due to the decomposition of similar compounds that have similar structures. However, it was found that each of the terminal groups showed slightly different large intervals in their decomposition temperatures (ΔT) and the highest maximum rates of mass loss (T_{max}). Each of the system is composed of the same repeated unit with different terminal groups, suggesting the drive towards decomposition with different kinetic stabilities. Then, the E_a of each system was obtained via the three aforementioned methods.

4.2. Calculation of Thermal degradation kinetics parameters

The E_a for the thermal degradation process of three different terminal groups was determined using three well-known methods for dynamic heating experiments, i.e. F-W-O, Kissinger, and C-Red methods. To apply the isoconversional method to F-W-O method from Eq. (7), the thermal decompositions of each terminal group of HPI were

scanned at different βs. α = 0 and α = 1 were taken at 100 °C and 800 °C, respectively. The E_a of different terminal groups of HPI was determined from a linear fitting of log β versus 1000/ T at different α (**Fig. 5a-c**).

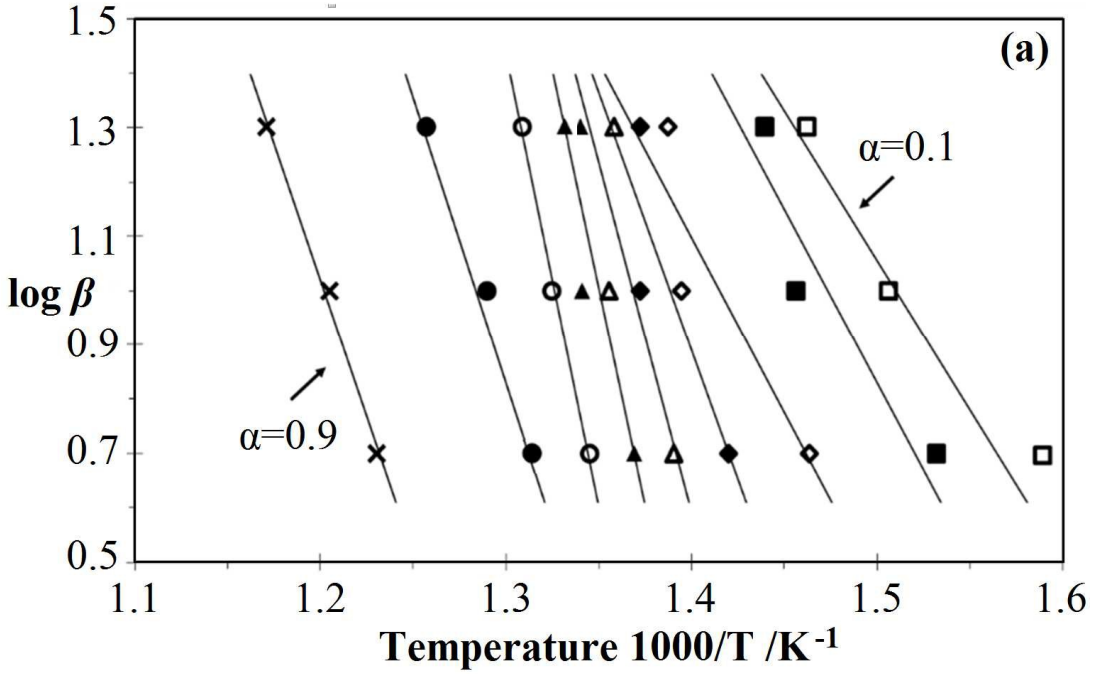

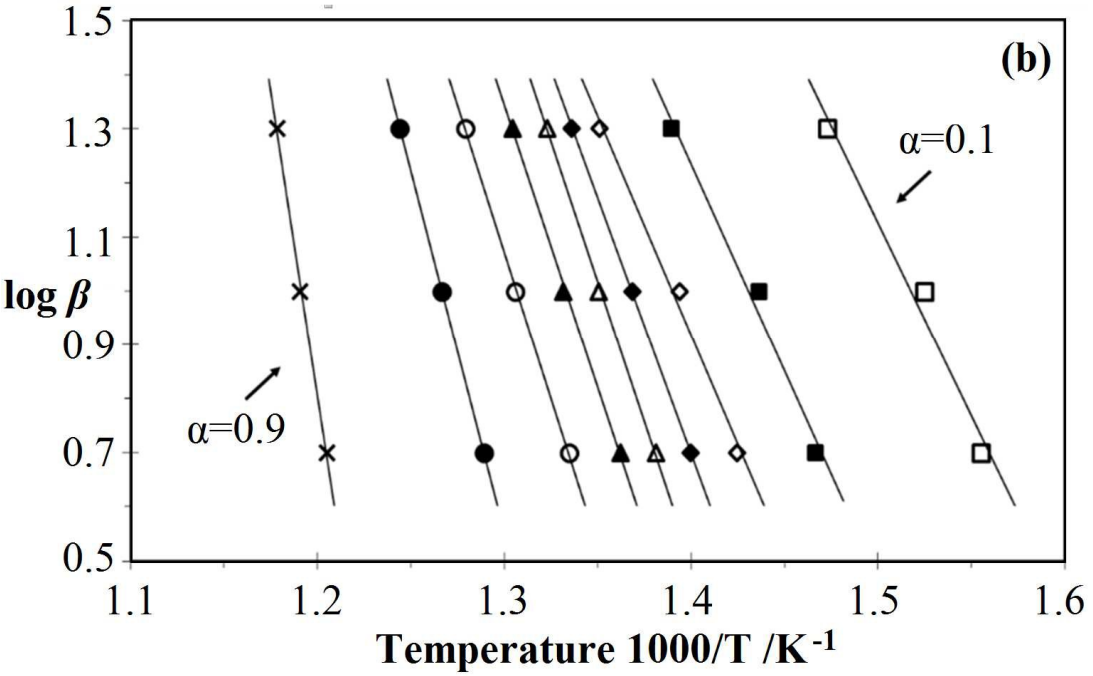

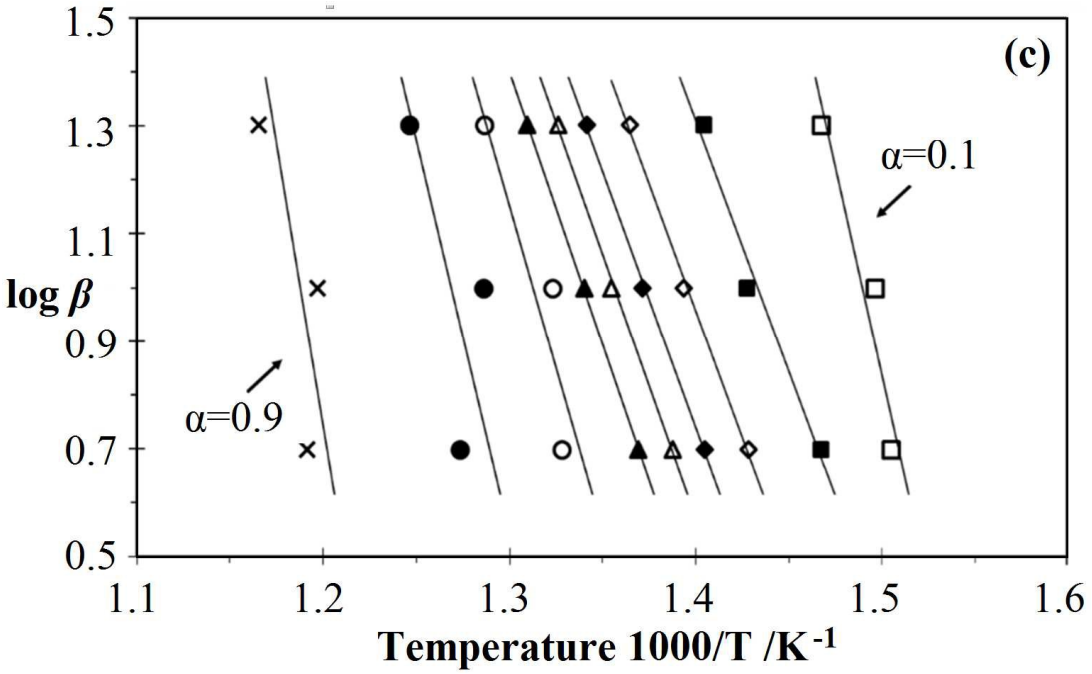

Fig. 5. Plot of log β versus 1000/T at different βs according to F-W-O method for (a) anhydride-amine terminated, (b) amine terminated and (c) anhydride terminated

From **Fig. 5a-c** the plot of log β versus 1000/T at different βs, it was found that the gradient obtained is a negative E_a. By following an approximately exponential relationship so that the rate constant could still be fitted to an Arrhenius expression, a negative value of E_a was obtained. This means that the rates of degradation decrease with the increase in temperature. Further increase of temperature leads to a reduced probability of the colliding molecules capturing one another. The summary and comparison of HPI derived from different terminal groups are shown in **Fig. 6**.

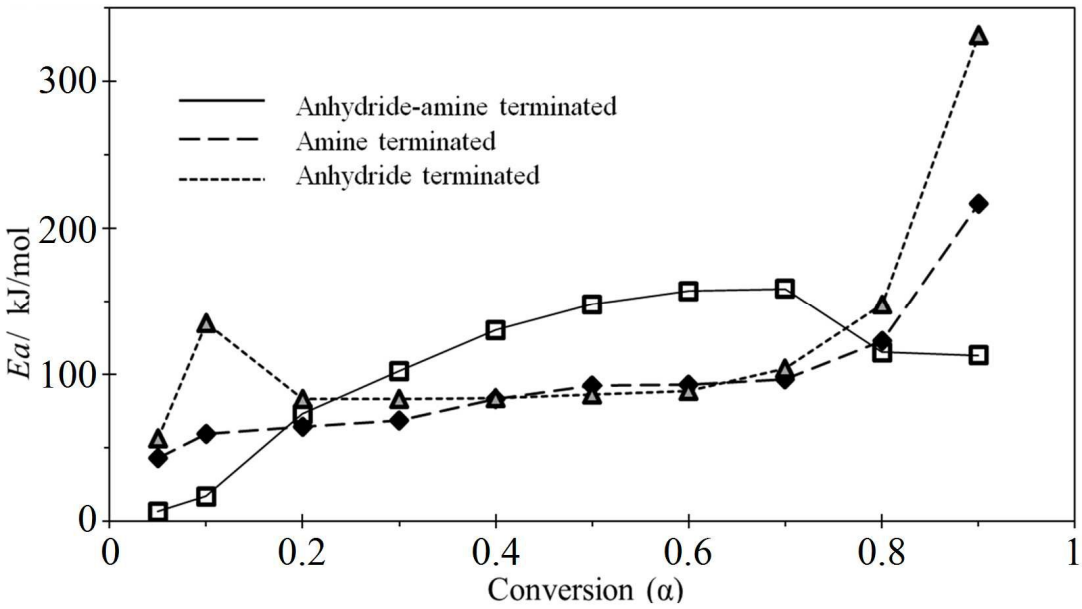

Fig. 6. Plot of E_a versus α according to F-W-O method for different terminal groups of melamine HPI

Fig. 6 shows the plot the dependence E_a on conversion, which is obviously indicated by the presence of a multi-step process. However**,** in our study, two stages of E_a have been determined, where the 1st stage of E_a behavior occurred at $\alpha < 0.7$and the 2nd stage started at $\alpha > 0.7$. At the 1st stage, the E_a increased moderately throughout the degradation process. These degradation kinetics are associated with the breaking of weak links. In general, for our study, the degradation is probably due to the breakdown of the aliphatic segment of propylidene bridge (C-$(CH_3)_2$) from B2 units or it could also be attributed to the weak bond that may exist (-NH-and -CONH-) between the side chain substituents, which are the weakest linkages along the polymer's main chain. This trend is similar to the results that have been reported by Tiptipakorn *et al*. [33] and Torrecillas *et al.* [34]. At the 2nd stage, as these weak links are consumed, the limiting step of degradation shifts towards the degradation initiated by random scission. This type of degradation requires higher levels of energy. Initially, the amine-terminated and anhydride0terminated HPI had demonstrated almost similar values and trends of E_a. However, once $\alpha > 0.7$, the

anhydride-terminated sample demonstrated a higher E_a compared to the amine-terminated sample. This distinction can be explained by comparing the dissociation energy between the anhydride functional groups (ΔH° C=O = +805 kJmol^{-1}) and amine functional groups (ΔH° N-H = +393 kJmol^{-1}).

Note that not every bond broken in the polymer chain leads to the evaporation of the product formed. However, there is also the possibility that a new bond formation has occurred. At $\alpha > 0.7$, the anhydride-amine terminated HPI sample which consisted of a dual-functional group showed a declining trend of E_a. This constitutes as evidence for the mentioned possibility, since the formation of a new bond requires lower E_a for the reaction. Thus, it is suggested that the amine-end and anhydride-end have reacted at high temperatures.

Due to the fact that Eq. (7) was derived from Doyle approximations, only α values in the low range can be used. In this study, the α values of 5 %, 10 %, 15 %, 20 %, 25 %, and 30 % were used. **Fig. 5a-c** shows that the fitted straight lines were almost parallel. Using F-W-O method, the E_a values corresponding to different α are listed in **Table 4**. The calculated E_a from this method are 51.31, 71.35, and 90.35 kJmol^{-1} for anhydride-amine, amine and anhydride terminated, respectively.

Table 4
E_a at α < 30 obtained using F-W-O method E_a at α < 30 obtained using F-W-O method

α	***E*$_a$ (kJ/mol)**	***R*^{2}**	**α**	***E*$_a$ (kJ/mol)**	***R*^{2}**	**α**	***E*$_a$ (kJ/mol)**	***R*^{2}**
Anhydride-amine terminated			Amine terminated			Anhydride terminated		
5	65.4	0.8098	5	43.27	0.8033	5	56.20	0.8439
10	16.93	0.7270	10	71.60	0.9787	10	107.45	0.9108
15	49.95	0.8011	15	79.07	0.9883	15	95.62	0.9237
20	63.90	0.6692	20	76.67	0.9837	20	93.90	0.9780

25	77.62	0.9769	25	76.55	0.9810	25	94.99	0.9914
30	92.90	0.9624	30	80.92	0.9919	30	93.93	0.9969
Average	51.31		Average	71.35		Average	90.35	

The E_a derived using Kissinger method can be calculated using the slope of the plot of ln (β/T_p^2) versus $1000/T_p$ (T_p is the temperature at the maximum mass-loss rate) as presented in **Fig. 7**. The plot for E_a versus α according to Kissinger method for different terminal groups of melamine HPI is shown in **Fig. 8**. From previous literature [35, 36], Kissinger method has been reported to provide highly reliable values of E_a with an error of less than 5%, independent of reaction mechanism, provided that E_a /RT > 10.

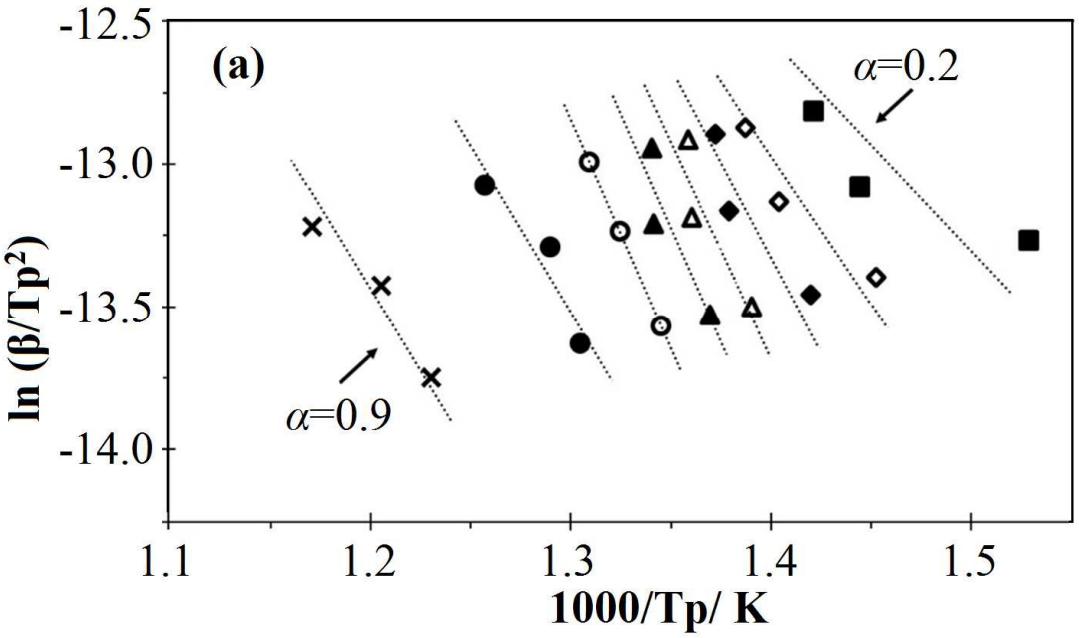

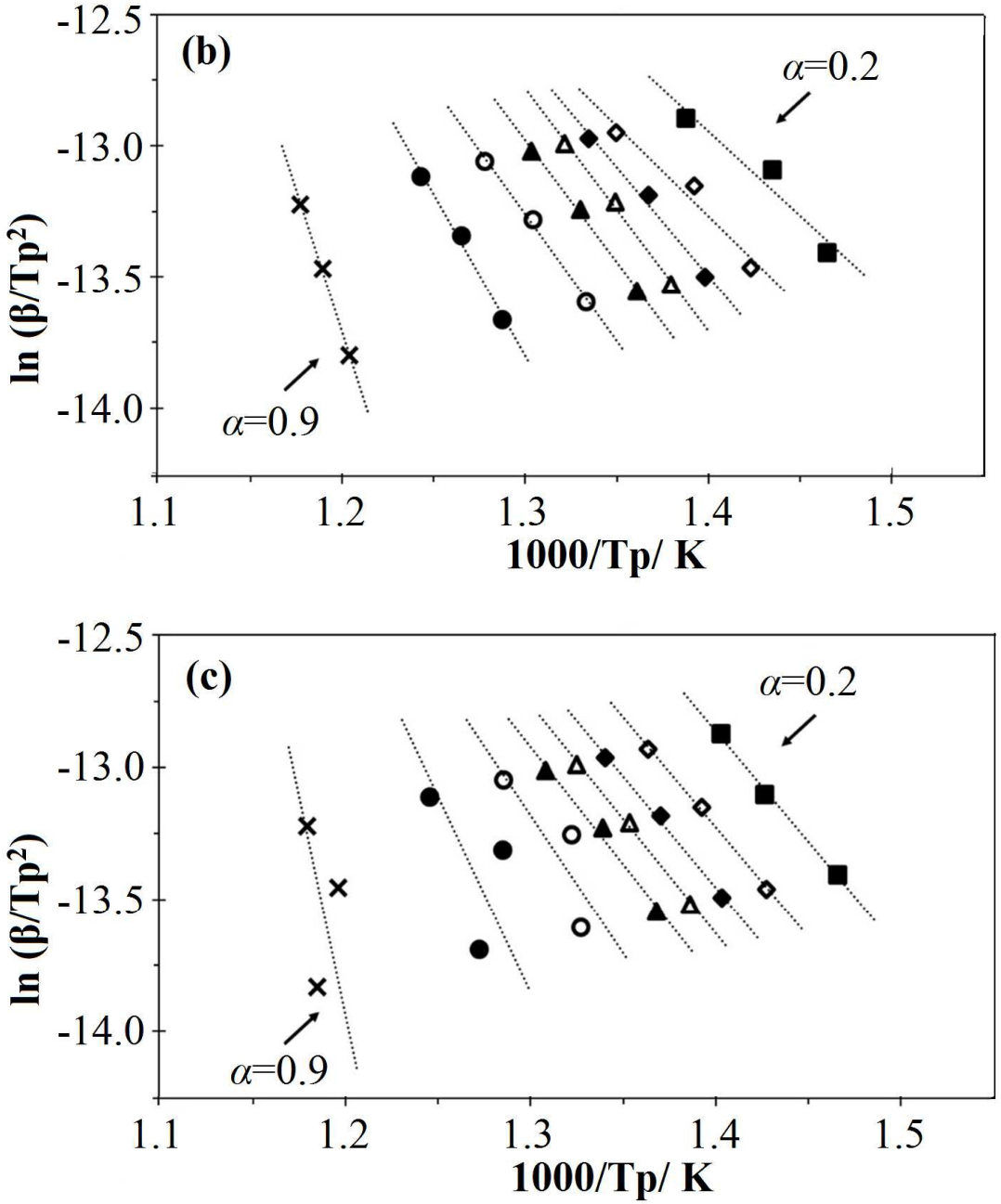

Fig. 7. Plot of ln β/Tp^2 at different βs according to Kissinger method for (a) anhydride-amine terminated, (b) amine terminated and (c) anhydride terminated

The calculated E_a (**Fig. 6** and **Fig. 8**) was found to have almost similar gradient and trends with F-W-O method. Thus, the results showed a negative value of E_a, which corresponds to the decrease in degradation rates in response towards the increase in temperatures. By following an approximately exponential relationship between F-W-O

and Kissinger methods, the rate constant can still be fitted to the Arrhenius expression. Therefore, **Table 5** shows the comparison of E_a versus α between F-W-O and Kissinger methods for different terminal groups of melamine HPI.

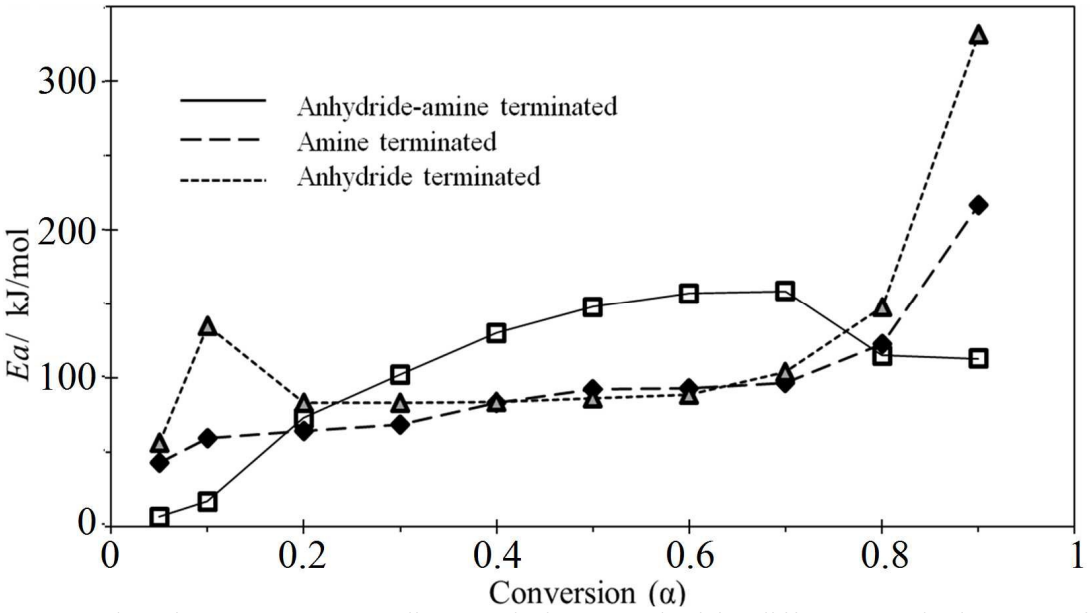

Fig. 8. Plot of Ea versus α according to Kissinger method for different terminal groups of melamine HPI

Table 5.
Comparison of E_a versus α between F-W-O and Kissinger methods for different terminal groups of melamine HPI.

F-W-O			Kissinger Method		
α	E_a (kJ/mol)	R^2	α	E_a (kJ/mol)	R^2
Anhydride-amine terminated HPI					
0.2	63.9	0.7692	0.2	73.0	0.7520
0.3	92.9	0.7624	0.3	102.2	0.7382
0.4	116.5	0.7711	0.4	130.3	0.7027
0.5	140.1	0.7804	0.5	148.0	0.8008
0.6	160.2	0.8732	0.6	157.2	0.9999
0.7	165.8	0.9939	0.7	158.5	0.8172
0.8	105.7	0.9420	0.8	115.0	0.8869
Amine terminated HPI					
0.2	76.7	0.9837	0.2	9.9	0.9326
0.3	80.9	0.9919	0.3	68.4	0.9539
0.4	94.7	0.9998	0.4	82.9	0.9852
0.5	103.4	0.9992	0.5	92.2	0.9949
0.6	104.4	0.9986	0.6	93.0	0.9965

0.7	108.2	0.9995	0.7	96.6	0.9941
0.8	134.1	0.9998	0.8	122.5	0.9892
		Anhydride terminated HPI			
0.2	93.9	0.9780	0.2	83.4	0.9951
0.3	93.9	0.9969	0.3	83.0	0.9985
0.4	95.0	0.9992	0.4	83.7	0.9951
0.5	97.7	0.9986	0.5	86.4	0.9964
0.6	100.4	0.9998	0.6	88.6	0.9855
0.7	120.4	0.8378	0.7	104.1	0.8155
0.8	214.8	0.8595	0.8	147.7	0.8243

It is clearly observed that the resulting E_a curve computed using both F-W-O and Kissinger methods has a similar change trend. Thus, this explains the fact that both these methods adhere to each other. However, the E_a values obtained from F-W-O method are higher than the values obtained from Kissinger method. This is because β in ln β/T (Eq. 8) depends on the function of temperature compared to log β in Eq. 7.

Remarkably, there are possible interactions or reactions that occur among different terminal groups of melamine HPI during degradation or among the products of degradation. Thus, these reactions can accelerate the degradation rate. As reviewed by Hamid *et al.* [37], the possible reactions might occur are between macromolecules and small molecules, macromolecules and small radicals, macroradicals and small molecules, two small molecules, two macroradicals or macromolecules and macroradicals. Note that the reactions with small molecules or small radicals can give rise to faster breakage of the macromolecules and to chemical structures that act as stabilizer groups. The above reasons can explain the phenomenon that happened to the amine-anhydride terminal group sample, in which E_a value decreased after α >0.7. These assumptions are not close to the predicted values on the basis of solid state processes. Thus, the most widely and accurately procedure to determine the possible reactions might occur has been proposed by Coats and Redfern [15, 16]. However, C-Red are designed to extract a single set of

Arrhenius parameters for the whole conversion ranges. The E_a for all $g(\alpha)$ functions can be obtained at constant β. Thus, **Table 6** lists the E_a obtained by using the C-Red method for several solid state processes at heating rate of 20 °Cmin^{-1} in nitrogen atmosphere.

Table 6.
E_a obtained using C-Red method for several solid state processes at β of 20 °Cmin^{-1} in nitrogen atmosphere.

Type	E_a (kJ/mol)	R^2	Type	E_a (kJ/mol)	R^2	Type	E_a (kJ/mol)	R^2
Anhydride-amine terminated HPI			Amine terminated HPI			Anhydride terminated HPI		
A2	64.26	0.9828	A2	40.90	0.9365	A2	44.14	0.9858
A3	38.90	0.9795	A3	23.27	0.9163	A3	25.44	0.9818
A4	26.1	0.9750	A4	14.46	0.8846	A4	16.04	0.9754
R1	242.76	0.9902	R1	166.19	0.9707	R1	175.92	0.9977
R2	127.61	0.9886	R2	85.13	0.9610	R2	90.70	0.9941
R3	131.61	0.9877	R3	87.96	0.9575	R3	93.78	0.9925
D1	**115.48**	**0.9911**	**D1**	**77.15**	**0.9743**	**D1**	**81.97**	**0.9979**
D2	258.06	0.9903	D2	176.50	0.9688	D2	187.14	0.9961
D3	275.11	0.9887	D3	187.89	0.9621	D3	199.61	0.9932
D4	263.72	0.9898	D4	180.24	0.9666	D4	191.30	0.9952
F1	140.42	0.9853	F1	93.86	0.9500	F1	100.26	0.9886
F2	42.23	0.7992	F2	24.19	0.6105	F2	27.51	0.7343
F3	96.35	0.8311	F3	18.87	0.7069	F3	67.09	0.8020

In this study, the same α values were used as those used in F-W-O and Kissinger methods. It was found that the solid state thermal degradation mechanism of the melamine derivative HPI is likely to be of D1 type, because this mechanism presents an E_a that is similar to the value obtained by isoconvensional methods. Furthermore, in comparison with other mechanisms, this mechanism renders the lowest E_a to start the degradation stage. The type of degradation mechanism is confirmed by using the Criado method in the next determination. As presented in **Table 7,** the C-Red method was applied for β values of, 5, 10, and 20 °Cmin^{-1} to determine the average values of E_a, A, and the degradation mechanism.

Table 7

E_a obtained using C-Red method at 5, 10, and 20 °Cmin^{-1} for different terminal groups of melamine HPI

β (℃/min)	E_a (kJ/mol)	ln A (/min)	R^2	Possible mechanism
Anhydride-amine terminated HPI				
5	20.95	10.0	0.9887	D1
10	76.73	1.45	0.9892	D1
20	118.64	5.90	0.9886	D1
Average	**72.11**			
Amine terminated HPI				
5	64.59	3.19	0.9887	D1
10	64.26	3.53	0.9888	D1
20	74.32	2.23	0.9661	D1
Average	**67.73**			
Anhydride terminated HPI				
5	98.77	2.66	0.9830	D1
10	82.64	0.47	0.9953	D1
20	81.06	1.04	0.9974	D1
Average	**87.49**			

The *Ea* values calculated using C-Red method are 72.11, 67.73 and 87.49 kJmol^{-1} where those values are almost comparable with the values that been obtained in Table 4 and Table 5 at low conversion (based on Doyle approximation). It is shown that most E_a for each degradation increased with the increase of β. In addition, the results suggest a D1 type of solid state thermal degradation mechanism for all different terminal groups of melamine HPI and all β. The possible reason of the simultaneous increase of E_a with the increase in β is due to the increase of the induced thermal stress to attain a thermodynamic equilibrium. Thus, the calculated E_a value is an average value of each β that corresponds to the area under the curve. The anhydride terminated sample has demonstrated a higher average of E_a than the amine terminated sample. Again, this distinction is due to the dissociation energy between the C=O bond (+805 kJmol^{-1}) and N-H bond (+393 kJmol^{-1}). It is clear that the bond dissociation energy mentioned is stronger than the calculated E_a. To adapt to this contrast, we propose that the decomposition of

different terminal groups of melamine HPI derivatives could be governed mainly by the molecular structure and kinetic consideration, and not fully by bond energy.

4.3 Determination of reaction mechanism using Criado method

The *Z(α)* master curves can be plotted using Eq. (13) according to different reaction mechanisms shown in **Table 1**. The experimental data at 20 °Cmin^{-1} obtained using F-W-O method (**Table 4**) were substituted into Eq. (14), while the calculated *dα/dT* curve is shown by **Fig. 9 (a, b)**. From the value obtained by **Fig. 9**, the *Z(α)* master and experimental curve of the different terminal groups of melamine HPI are plotted (**Fig. 10**).

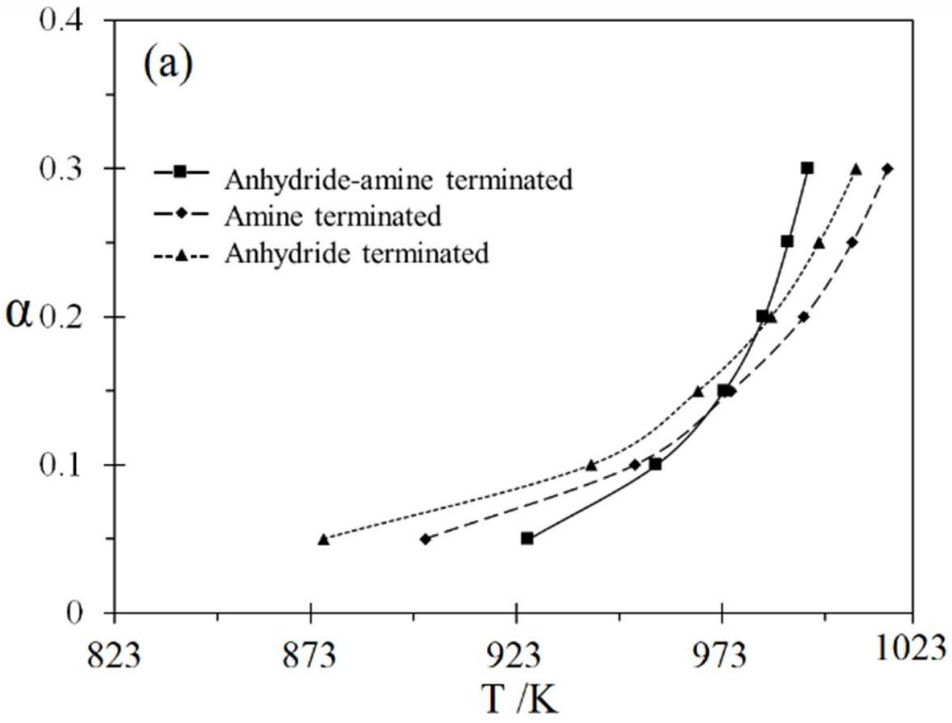

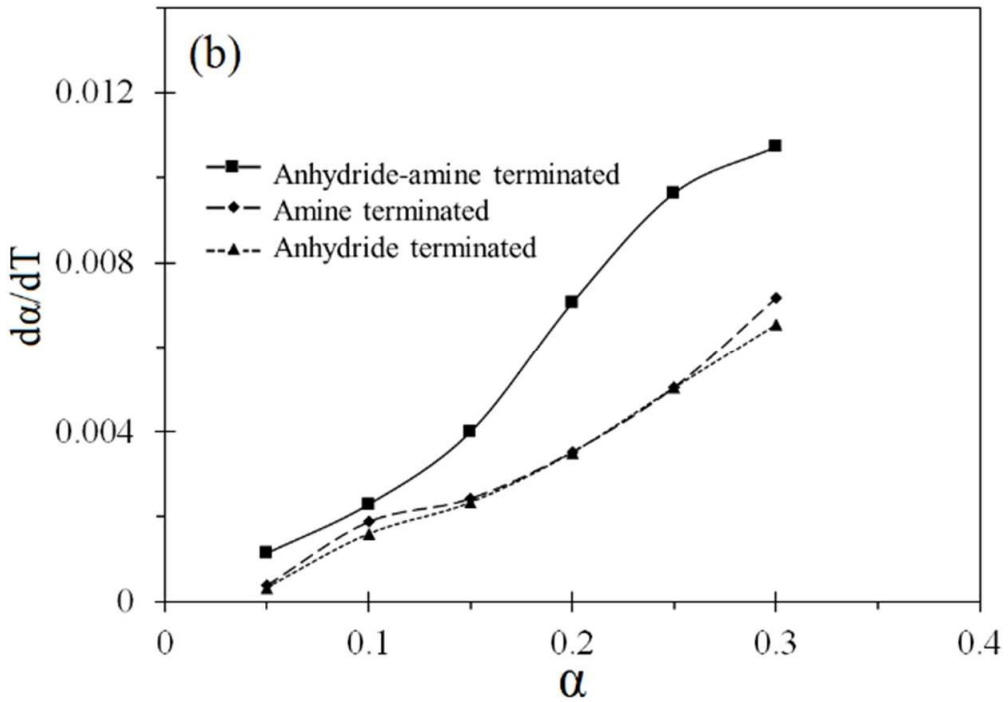

Fig. 9. Plot of α versus temperature (**a**) and $d\alpha/dT$ versus α (**b**) according to F-W-O method.

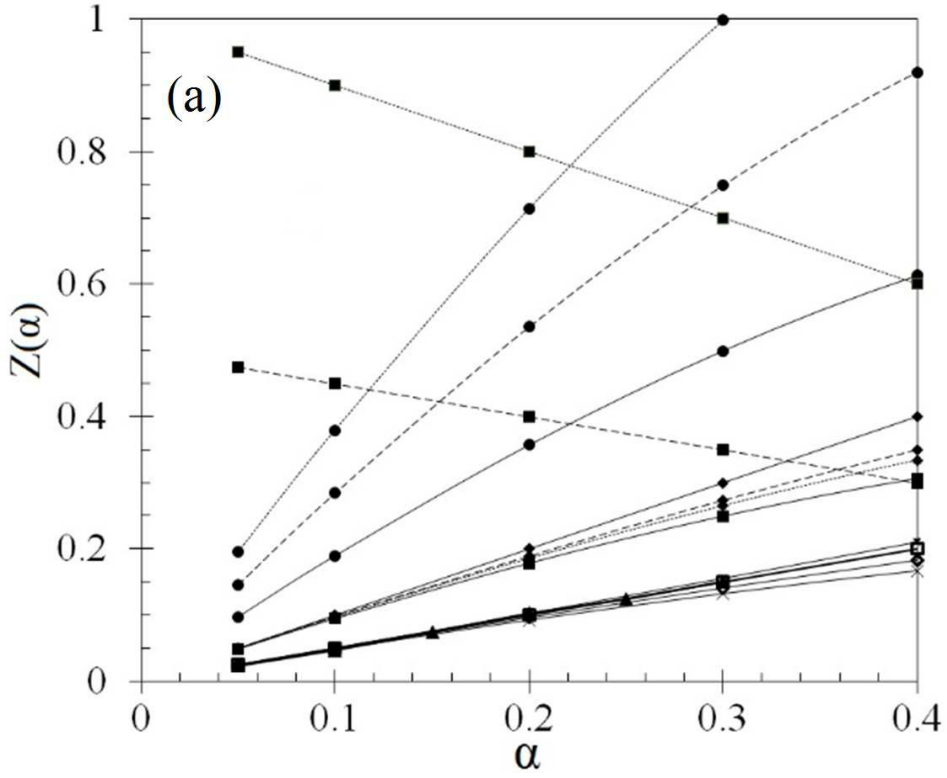

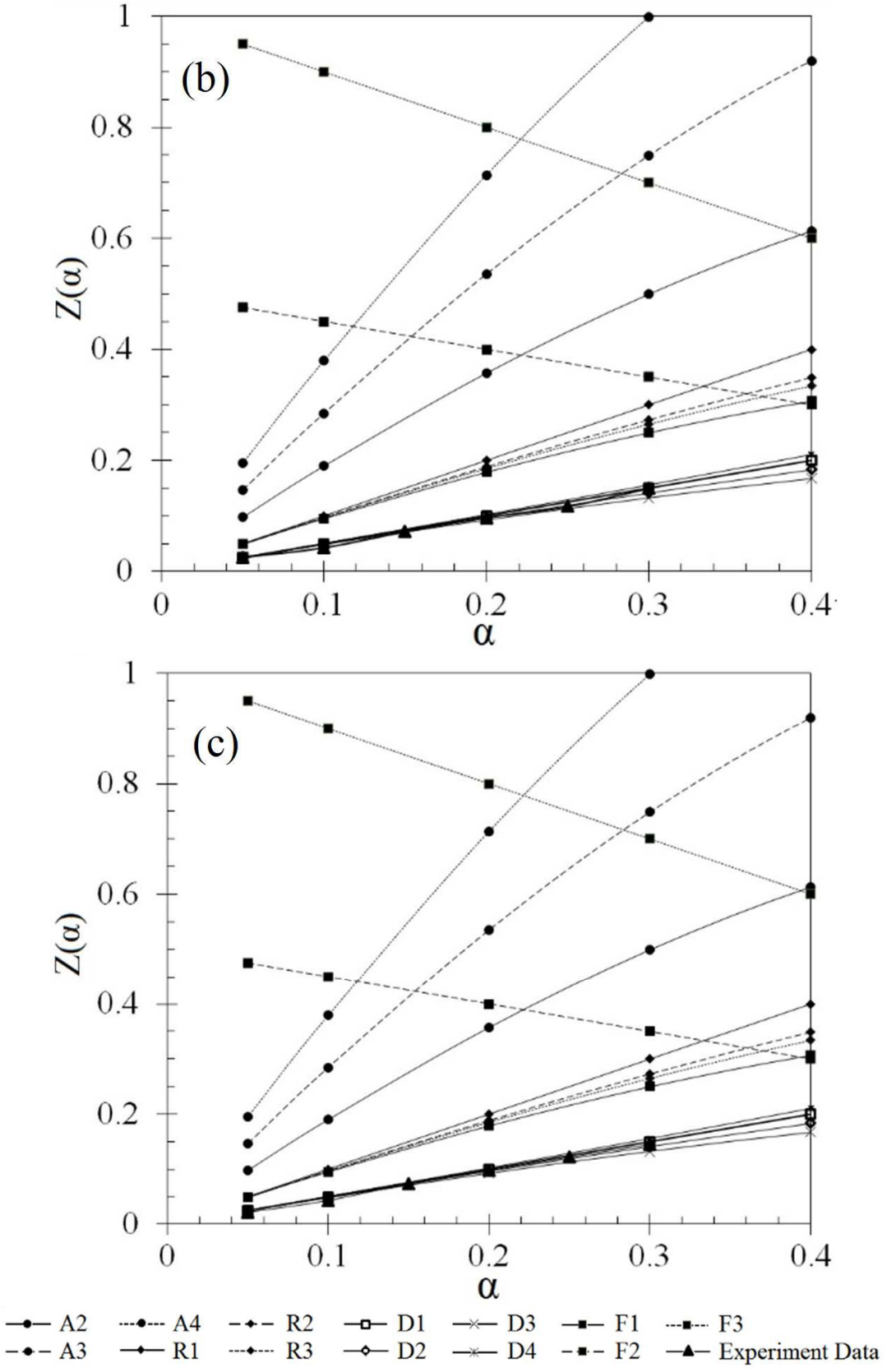

Fig. 10. Plot of $Z(\alpha)$ versus α HPI between the experimental curve and master curve of different mechanisms for **(a)** anhydride-amine terminated, **(b)** amine terminated and **(c)** anhydride terminated.

Fig. 10 (a, b, and **c)** exhibit the comparison of the experimental curves and master curves, respectively. The results showed that the experimental curves of all degradations belong to the D1 reaction mechanism (one-dimensional diffusion) with rate controlling step of the diffusion process. That means the degradation is initiated from one random point (i.e. from one terminal group to the main and chain vice versa) where it is follows the unimolecular decay law with the first order reaction based on the Fick's first law (by assuming the diffusion coefficient represents the proportionality constant between the particle flux and the concentration gradient)[38]. Therefore, this can be described the degradation point move between PI chains which are separated by a distance to the other neighbouring PI chains in plane. Further degradation in PI chain may move from one chain to its neighbouring chain at certain specific of moving frequency. The degradation chain points have an equal probability of moving to other neighbouring chain in the opposite direction. The total number of degradation moving out to other chain per unit time is equal to the decomposed number of PI chain per unit area. The movement between degradation points to other neighbouring point could be understood as vacancy or interstitially phenomena.

4.4. Lifetime Prediction

Lifetime estimation is also very useful in the development, design and selection process of polymers for different applications. The apparent kinetic parameters calculated from this study have been used to obtain the lifetime of formulated microgel systems. The estimated lifetime of a polymer until failure has been defined as the time when the mass

loss reaches 5 wt% (α = 0.05). By substituting Eq. 4 into Eq.6, Eq. 13 is produced. From the integration, the lifetime can be estimated using Eq. 14 or Eq. 15:

$$\frac{d\alpha}{dt} = A\exp\frac{Ea}{RT}(1-\alpha)^n \qquad (14)$$

$$t_f = \frac{(1-0.95^{1-n})}{A(1-n)}\exp\frac{Ea}{RT} \qquad (n\neq 1) \qquad (15)$$

$$t_f = \frac{0.0513}{A}\exp\frac{Ea}{RT} \qquad (n=1) \qquad (16)$$

The value of η can be obtained directly from the symmetrical index of a DTG peak, based on the second Kissinger technique, which is demonstrated in Eq. 16:

$$n = 1.88\frac{\left[\frac{d^2\alpha}{dt^2}\right]_L}{\left[\frac{d^2\alpha}{dt^2}\right]_R} \qquad (17)$$

where the indices L and R correspond to the left and right peak ($d^2\alpha/dt^2$) values respectively, on the second derivative thermogravimetric (DDTG) curve for the decomposition process. The values of n and *ln* A for the decomposition in nitrogen atmosphere are listed in **Table 8** and the results for lifetime as a function of service temperature of different terminal groups of melamine HPI in nitrogen atmosphere shows in **Fig. 11**

Table 8
Results for kinetic degradation parameters and lifetime as a function of service temperature of different terminal groups of melamine HPI in nitrogen atmosphere

Sample Designation	n [a]	Ea [b] *J/mol*	Life time predications [c]				
			25 °C	100 °C	250 °C	500 °C	1000 °C
Anhydride-amine terminated,	0.9	36549	$2.6x10^{5}$	$1.3x10^{4}$	$4.0x10^{2}$	$2.5x10^{1}$	$0.2x10^{1}$
Amine terminated	0.9	43267	$5.0x10^{6}$	$1.4x10^{5}$	$2.3x10^{3}$	$8.6x10^{1}$	$0.5x10^{1}$
Anhydride terminated.	0.9	56196	$8.0x10^{9}$	$1.3x10^{7}$	$6.3x10^{4}$	$8.7x10^{2}$	$1.3x10^{1}$

[a] Kinetic order, [b] Activation energy in J/mol, [c] lifetime (hour) predications of service temperature in ,

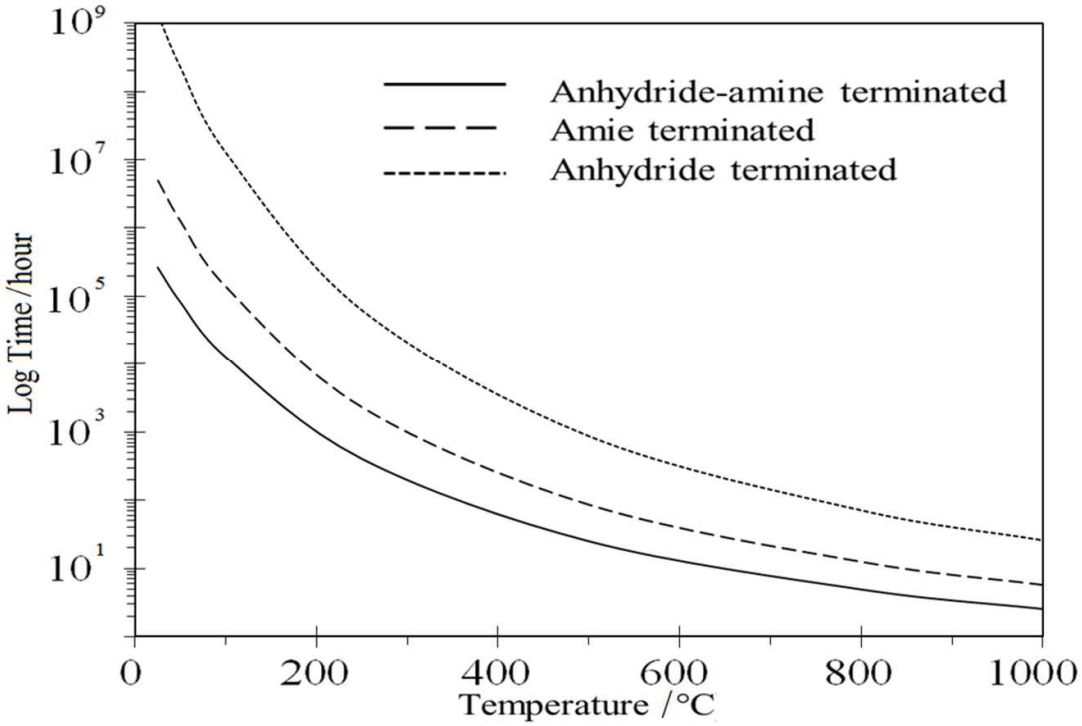

Fig. 11. Lifetime as a function of service temperature in the presence of different terminal groups of melamine HPI in nitrogen atmosphere

In nitrogen atmosphere, the lifetime predicted for all different terminal groups of melamine HPI system used the assumption of pseudo-first order reaction kinetics with an exponential curve. It could be observed that the lifetime was strongly dependent on the service temperature, and decreased significantly as the temperature increased from 25 °C

to 500 °C. It is suggested that the temperature supplies energy to increase chain mobility and rate of degradation, while shortening its lifetime. Besides that, it was found that the lifetime decreased in the following order: anhydride terminated>amine terminated>anhydride-amine terminated. Again, this distinction is related to the dissociation energy between the anhydride functional groups (ΔH^o C=O = +805 kJmol^{-1}) and amine functional groups (ΔH^o N-H = +393 kJmol^{-1}). Note that this contradicts with the anhydride-amine terminated HPI sample that consists of a dual functional group, since the formation of new bonds requires a lower E_a for the reaction. However, the kinetics of the degradation process depends strongly on chain mobility, which further depends on the physical state of the polymer. Chain mobility is much higher in the molten state than in the solid state, thereby making the predictions even more inaccurate for the solid state.

4. Conclusions

Although different terminal groups did not show significant changes on TG curves, yet the curves did not overlap each other. Thus, their contribution towards kinetic parameters and solid state during thermal degradation will be the points to be evaluated in this study. The TG curve shifted to higher temperatures as β increased, which is due to the inducement of thermal stress in order to attain thermodynamic equilibrium. The resulting E_a curves computed using both F-W-O and Kissinger methods have similar change trends, thus, both methods adhere to each other. It was found that the E_a and lifetime obtained adhered to the following order; anhydride terminated>amine terminated>anhydride-amine terminated. This distinction is related to the dissociation energy between the anhydride functional groups (ΔH^o C=O = +805 kJmol^{-1}) and amine functional groups (ΔH^o N-H = +393 kJmol^{-1}). Note that this contradicts to the anhydride-amine terminated HPI sample that consists of a dual-functional group, since the formation

of new bonds requires a lower E_a for the reaction. As Calculated, the degradation of amine-amine terminal, amine-anhydride terminal and anhydride-anhydride terminal HPI follows the D1 thermal degradation mechanism in the α range, which is considered as a one-dimensional diffusion that follows the unimolecular decay law of the first order reaction.

Acknowledgements

The authors wish to acknowledge Universiti Sains Malaysia for sponsoring this project under FRGS-203/PBAHAN/6071242 and USM-RU-PGRS-1001/PBAHAN/8046027, as well as School of Material and Mineral Source Engineering and the USM Engineering Campus for their technical support.

References

1. C. Gao and D. Yan, *Progress in Polymer Science*, 2004, **29**, 183-275.
2. G.-A. Wen, Y. Xin, X.-R. Zhu, W.-J. Zeng, R. Zhu, J.-C. Feng, Y. Cao, L. Zhao, L.-H. Wang and W. Wei, *Polymer*, 2007, **48**, 1824-1829.
3. S. S. Mahapatra and N. Karak, *Journal of applied polymer science*, 2007, **106**, 95-102.
4. X. Peng, Q. Wu, S. Jiang, M. Hanif, S. Chen and H. Hou, *Materials Letters*, 2014, **133**, 240-242.
5. F. C. Rauch and A. J. Fanelli, *The Journal of Physical Chemistry*, 1969, **73**, 1604-1608.
6. M. Yang, D. Wang, N. Sun, C. Chen and X. Zhao, *High Performance Polymers*, 2014, 0954008314555521.
7. A. Ghosh, S. Banerjee and B. Voit, *Advances in Polymer Science*, 2015, **266**, 27-124.
8. S. Vyazovkin and C. A. Wight, *Thermochimica acta*, 1999, **340**, 53-68.
9. T. Ozawa, *Journal of Thermal Analysis and Calorimetry*, 1970, **2**, 301-324.
10. T. Ozawa, *Bulletin of the chemical society of Japan*, 1965, **38**, 1881-1886.
11. J. H. Flynn, *Thermochimica Acta*, 1997, **300**, 83-92.
12. H. E. Kissinger, *Analytical chemistry*, 1957, **29**, 1702-1706.
13. H. E. Kissinger, *Journal of Research of the National Bureau of Standards*, 1956, **57**, 217-221.
14. A. Coats and J. Redfern, *Nature*, 1964, **201**, 68 - 69.
15. A. Coats and J. Redfern, *Journal of Polymer Science Part B: Polymer Letters*, 1965, **3**, 917-920.
16. A. Coats and J. Redfern, *Analyst*, 1963, **88**, 906-924.
17. H. H. Horowitz and G. Metzger, *Analytical Chemistry*, 1963, **35**, 1464-1468.
18. J. MacCallum and J. Tanner, *Nature*, 1970, **225**, 1127-1128.
19. J. MacCallum and J. Tanner, *European Polymer Journal*, 1970, **6**, 1033-1039.
20. D. W. Van Krevelen and K. Te Nijenhuis, *Properties of polymers: their correlation with chemical structure; their numerical estimation and prediction from additive group contributions*, Elsevier, 4 edn., 2009.
21. H. L. Friedman, 1964.
22. J. Criado, J. Malek and A. Ortega, *Thermochimica Acta*, 1989, **147**, 377-385.
23. J. Criado, L. Pérez-Maqueda, F. Gotor, J. Málek and N. Koga, *Journal of thermal analysis and calorimetry*, 2003, **72**, 901-906.

24. L. Perez-Maqueda, J. Criado, F. Gotor and J. Malek, *The Journal of Physical Chemistry A*, 2002, **106**, 2862-2868.
25. C. D. Doyle, *Journal of Applied Polymer Science*, 1961, **5**, 285-292.
26. C. Doyle, *Journal of applied polymer science*, 1962, **6**, 639-642.
27. C. D. Doyle, *Nature*, 1965, **207**, 290-291.
28. M. B. H. Othman, R. Ramli, Z. M. Ariff, H. M. Akil and Z. Ahmad, *J Therm Anal Calorim*, 2012, **109**, 1515-1523.
29. W. L. Paterson, *Journal of Computational Physics*, 1971, **7**, 187-190.
30. G. Senum and R. Yang, *Journal of thermal analysis*, 1977, **11**, 445-447.
31. M. B. H. Othman, H. M. Akil, H. Osman, A. Khan and Z. Ahmad, *Journal of Thermal Analysis and Calorimetry*, 2015, 1-14.
32. W. Xie and W. P. Pan, *Journal of Thermal Analysis and Calorimetry*, 2001, **65**, 669-685.
33. S. Tiptipakorn, S. Damrongsakkul, S. Ando, K. Hemvichian and S. Rimdusit, *Polymer Degradation and Stability*, 2007, **92**, 1265-1278.
34. R. Torrecillas, A. Baudry, J. Dufay and B. Mortaigne, *Polymer Degradation and Stability*, 1996, **54**, 267-274.
35. J. Criado and A. Ortega, *Journal of non-crystalline solids*, 1986, **87**, 302-311.
36. L. Barral, J. Cano, J. Lopez, I. Lopez-Bueno, P. Nogueira, C. Ramirez and M. Abad, *Journal of thermal analysis and calorimetry*, 1998, **51**, 489-501.
37. A. M. Hamid SH, Maadhah AG., *Handbook of polymer degradation.*, Marcel Dekker, New York, 1992.
38. R. C. Ropp, *Solid State Chemistry*, Elsevier Science, 2003.